Journal of Materials Chemistry C

Inducing Planarity in Redox-Active Conjugated Polymers with Solubilizing 3,6-Dialkoxy-thieno[3,2-b]thiophenes (DOTTs) for Redox and Solid-State Conductivity Applications

Journal:	*Journal of Materials Chemistry C*
Manuscript ID	TC-ART-02-2020-000914.R1
Article Type:	Paper
Date Submitted by the Author:	10-Apr-2020
Complete List of Authors:	Pittelli, Sandra; Georgia Institute of Technology, Chemistry and Biochemistry Gregory, Shawn; Georgia Institute of Technology, Mechanical Engineering Ponder, James; Georgia Institute of Technology; Imperial College London Yee, Shannon; Georgia Institute of Technology, Mechanical Engineering Reynolds, John; Georgia Institute of Technology, Chemistryand Biochemistry, Materials Science and Engineering

Inducing Planarity in Redox-Active Conjugated Polymers with Solubilizing 3,6-Dialkoxy-thieno[3,2-*b*]thiophenes (DOTTs) for Redox and Solid-State Conductivity Applications

Sandra L. Pittelli[1], Shawn A. Gregory[2], James F. Ponder Jr.[3], Shannon Yee[4] and John R. Reynolds[1,2*]

[1]School of Chemistry and Biochemistry, [2]School of Materials Science and Engineering, Center for Organic Photonics and Electronics, Georgia Tech Polymer Network, Georgia Institute of Technology, Atlanta, GA, USA. E-mail: Reynolds@chemistry.gatech.edu

[3] Department of Chemistry, Imperial College of London, London, United Kingdom.

[4]George W. Woodruff School of Mechanical Engineering, Georgia Institute of Technology, Atlanta, GA, USA.

Abstract

In this work, we evaluate a series of dioxythienothiophene (DOTT)-based polymers for their charge transport structure-property relationships for both solid-state and electrochemical applications. The family includes: (i) the homopolymer, (ii) two 3,4-ethylenedioxythiophene (EDOT) co-polymers, (iii) a dimethyl ProDOT (DMP) co-polymer, and (iv) a bulky neopentyl dioxythiophene (NeoDOT) co-polymer. We show that all of the soluble DOTT polymers can be oxidized through chemical or electrochemical processes, through the full depletion of their neutral π-π^* absorbance. The DOTT homopolymer and DOTT-NeoDOT co-polymer show high degrees of intermolecular ordering according to GIWAXS measurements, however, this order inhibits both chemical and electrochemical oxidation. DOTT-NeoDOT has the highest onset of electrochemical oxidation at 0.3 V *vs.* Ag/Ag^+. In comparison, DOTT-BiEDOT has lower degrees of intermolecular ordering and the lowest onset of oxidation at -0.5 V *vs.* Ag/Ag^+. Furthermore, this polymer has the highest solid-state conductivity of the family, which

approaches 20 S/cm after chemical oxidation with the molecular dopant F4TCNQ. This study is the first to report the effects of chemical doping and charge transport on a family of soluble DOTT-based polymers.

1. Introduction:

Conjugated polymers (CPs) are desirable materials for a wide range of applications due to their ability to transport both ions and electrons simultaneously. They have been investigated as active materials in both solid-state and redox-active applications due to their ability to transition from a charge-neutral (insulating) state, to a charged (conducting) state through either chemical or electrochemical oxidation (doping). Solid-state applications, which capitalize on the electronic charge transport of CPs include radio frequency shielding (RFS) devices,[1-2] thermoelectric generators,[3-4] and transparent conductive electrodes (TCEs).[5-7] Redox-active applications require the transport of both electronic and ionic charge and some polymer applications include: electrochromic devices (ECDs),[8-9] supercapacitors,[10-11] and organic electrochemical transistors (OECTs).[12-13] Though there is diversity in the applications of CPs, all benefit from materials that can be oxidized and efficiently transport charge.

Significant effort has been expended establishing the foundation for understanding the structure-property relationships of CPs as they relate to the transport of electronic and ionic charge. In terms of solid-state applications, it has been shown that higher degrees of intermolecular ordering can lead to enhanced electrical conductivity[14-16] and charge transport in general,[17] however, there is still a question about how this degree of order can relate to ionic transport and electrochemical switching. Some work has suggested that high degrees of intermolecular ordering can lead to inhibited transport of ionic charge.[12, 18]

Furthermore, it has been shown that doping efficiency of CPs can be improved and electrical conductivities can be increased through the proper selection of a chemical oxidant (dopant).[19-20] The work presented by Scholes *et al.* demonstrated that the ability of the polymer microstructure to incorporate the molecular dopant can also govern the mobility of the generated carriers.[21] In terms of redox-active applications, work in the literature has shown that manipulation of the repeat unit of the polymer can affect properties such as the onset of oxidation,[22] redox capacity,[11, 23] and doping kinetics.[24] Alteration of the structure of the side chain of the polymer has also been shown to affect the degree of swelling during electrochemical doping and therefore ionic transport through the polymer film.[12, 25-26] In the field of bioelectronics in particular, there has been significant effort towards understanding the structure-property relationships of the mixed transport of ions and electrons, and how the morphology of solution-processed CP films can affect these charge transport properties.[27-29] Optimal polymer performance for all of these applications includes effective transport of both ionic and electronic charge.

Dioxythiophene (XDOT)-based materials are desirable active materials for use in both solid-state and redox-active applications. Recently, a soluble dioxythiophene polymer has been shown to have high solid-state conductivity after chemical doping (over 200 S/cm).[30] Polymers with repeat units based on 3,4-propylenedioxythiophene (ProDOT) are also effective active materials in electrochromic[31] and OECT applications.[32] Since 1986, thienothiophene (TT)-based materials have been investigated for their electrochemical properties.[33] Additionally, these fused materials have been shown to be highly conducting due to their increased degree of intermolecular ordering after chemical oxidation.[34-38] These materials have also demonstrated high degrees of crystallinity before chemical

oxidation and high mobilities.[39-40] A TT-based polymer with oligoether sidechains has been shown to exhibit an electrical conductivity on the order of 100 S/cm[41] and its hydrocarbon sidechain counterpart (PBTTT) has a high degree of intermolecular ordering.[42] Despite these advances, the effects of TT moieties on ionic charge transport in electrochemical devices has not yet been quantified.

Dioxythienothiophene (DOTT)-based polymers are a group of materials that combine the electron-rich nature of dioxythiophenes with a planar thienothiophene moiety. The work from Turbiez *et al.* in 2005 showed that an electrochemically polymerized DOTT homopolymer has electrochromic properties that are similar to those of poly(3,4-ethlenedioxythiophene) (PEDOT).[43] Since 2005, DOTTs have been shown to be effective redox-active materials in applications such as electrochromic[44-45] and charge storage devices,[46] however, the effects of the polymer structure on properties, such as the degree of intermolecular ordering and charge transport, have yet to be explored.

In this work, we gain a comprehensive understanding of how a DOTT moiety can affect the morphology and charge transport of a soluble CP family for use in both solid-state and redox-active applications. To achieve this, we evaluated a series of DOTT-based polymers which includes the homopolymer, two 3,4-ethylenedioxythiophene (EDOT) co-polymers, a dimethyl ProDOT (DMP) co-polymer, and finally a bulky neopentyl dioxythiophene (NeoDOT) co-polymer. In order to further understand the processes of chemical oxidation, we doped this family of polymers with either a bulky organic salt, Tris(4-bromophenyl)ammoniumyl hexachloroantimonate (commonly referred to as "Magic Blue") or planar electron-accepting organic molecule, 2,3,5,6-Tetrafluoro-7,7,8,8-tetracyanoquinodimethane (commonly referred to as F4TCNQ). To our knowledge, this is

the first time studies have been conducted on the chemical oxidation of DOTT CPs. We show that DOTT moieties in soluble CPs leads to increased degrees of intermolecular order, but that too much of this order inhibits both electronic charge transport and the ease of electrochemical oxidation. The DOTT homopolymer and DOTT-NeoDOT co-polymer show the highest degrees of intermolecular order in the family, but solid-state conductivities that are four orders of magnitude lower than the other polymers. Furthermore, the electrical conductivity of DOTT-BiEDOT is enhanced by two orders of magnitude, and approaches 20 S/cm after oxidation with the weaker, but more planar chemical oxidant F4TCNQ as compared to Magic Blue. Finally, it is shown that chemically oxidized DOTT polymers have enhanced air stability and retain up to 70% of their original conductivity after storage in ambient conditions for two weeks, as compared to the less stable highly investigated materials such as PBTTT.

2. Results and Discussion:

2.1 Approach

For this study, we designed and synthesized a unique family of polymers that incorporate a DOTT moiety as depicted in Scheme 1. All polymers were synthesized using direct (hetero)arylation polymerization. Details on the synthesis, purity, and molecular weights of these materials can be found in the Supporting Information. This data confirms the structures of these materials, as well as demonstrating that all of the materials in the family are above the effective conjugation length and the molecular weights are in a comparable range of 6-30 kg/mol. The nuclear magnetic resonance (NMR) data can be seen in Figures S1-4, and gel permeation chromatograms for each polymer can be seen in Figures S5-S9. DOTT was chosen due to its fused and planar structure, and suggestions

from work in the literature that this moiety would enhance inter-chain ordering and solid-state conductivity of the polymer in the doped and oxidized state.[37, 42, 47] In order to gain a holistic understanding of the structure-property relationships of the DOTT family, the homopolymer (Homo-DOTT, HD), as well as the four co-polymers were synthesized. Previous work showed that the incorporation of EDOT structures into the repeat unit of a soluble dioxythiophene polymer leads to increased solid-state conductivities after chemical oxidation.[30]

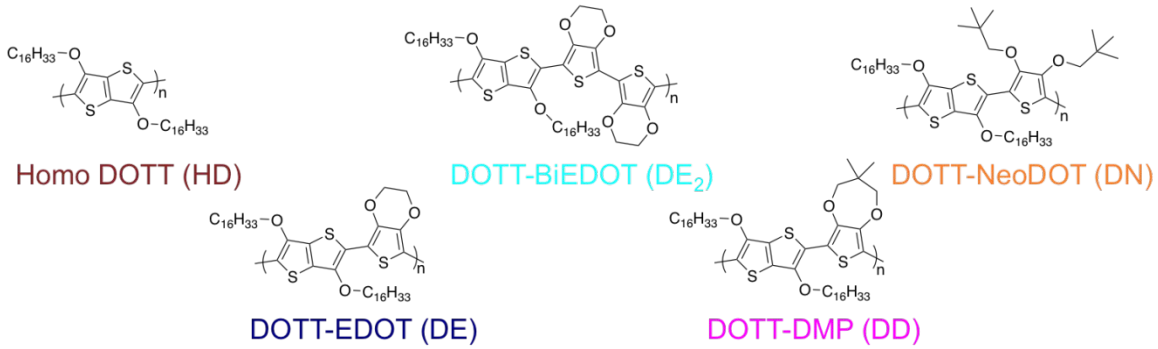

Scheme 1: Repeat unit structures of polymers used in this study. The $C_{16}H_{33}$ sidechains used here represent branched hexyldecyl chains.

The DMP unit was included following work showing that dioxythiophene polymers that incorporate the DMP moiety have fast switching kinetics.[24, 32] It has not yet been explored how both the EDOT and DMP moieties can affect properties such as the degree of intermolecular ordering and the interactions between molecular dopants and the polymer chains. Finally, the co-polymer DOTT-NeoDOT (DN) was included in this study in order to understand how the DOTT material properties would be affected by a sterically strained backbone. The neopentyl side chains substituted onto the dioxythiophene unit in NeoDOT provide increased steric bulk as compared to either the EDOT or DMP units, resulting in a

polymer that is expected to have a more twisted backbone relative to the other polymers in the family. Building from our previous work involving acyclic dioxythiophenes, this is expected to result in a polymer that is more difficult to oxidize than the rest of the family, and result in highly ordered polymer films.[48]

2.2 Characterization of Intermolecular Ordering

The degree of intermolecular ordering has been shown to have a large influence on the charge transport properties of CPs. One method for evaluating this property is Grazing-Incidence Wide-Angle X-ray Scattering (GIWAXS). GIWAXS measurements can show the degree and directionality of the polymer chain ordering relative to the sample substrate, and can also be used to extract interchain spacing distances. For this work, it is not only important to understand how the polymer repeat unit can affect the film morphology, but also how this morphology can be altered after doping with a molecular chemical oxidant and how this relates to the polymer film's electrical conductivity.

GIWAXS measurements were performed on blade-coated polymer films as shown in Figure 1. The scattering images reveal that the polymer backbone structure does have an effect on the degree of ordering and directionality of the polymer films. We see that Homo DOTT (Figure 1a), DOTT-BiEDOT (Figure 1c), and DOTT-DMP (Figure 1d) have preferential lamellar ordering (100) in along the Q_{xy} direction and preferential π-π stacking (010) along the Q_z direction, showing that the polymer chains are most ordered in-plane relative to the substrate. These trends are evidenced by the more narrow (100) peaks along the Q_{xy} direction as compared to the more diffuse (100) peaks along the Q_z direction. Q_z and Q_{xy} linecuts of all polymers can be seen in Figure S10.

Homo DOTT is the most highly ordered of the group (Figure 1a) as shown by the multiple signals along the Q_z and Q_{xy} axes relating to high degrees of lamellar ordering. It is hypothesized that the large number of scattering signals could be due to the presence of multiple polymorphs in the film, as many peaks are observed very close together. If no polymorphs were observed, we would expect for each of these peaks to occur at distances that are integer multiples of each other. DOTT-EDOT (Figure 1b) in contrast, is shown to be the least ordered of the group as evidenced by the halos in the (100) and (010) planes. This trend may be somewhat surprising, however, we hypothesize that because DOTT-EDOT has minimal steric bulk, the polymer chains can adopt many conformations which results in a more disordered film morphology overall.

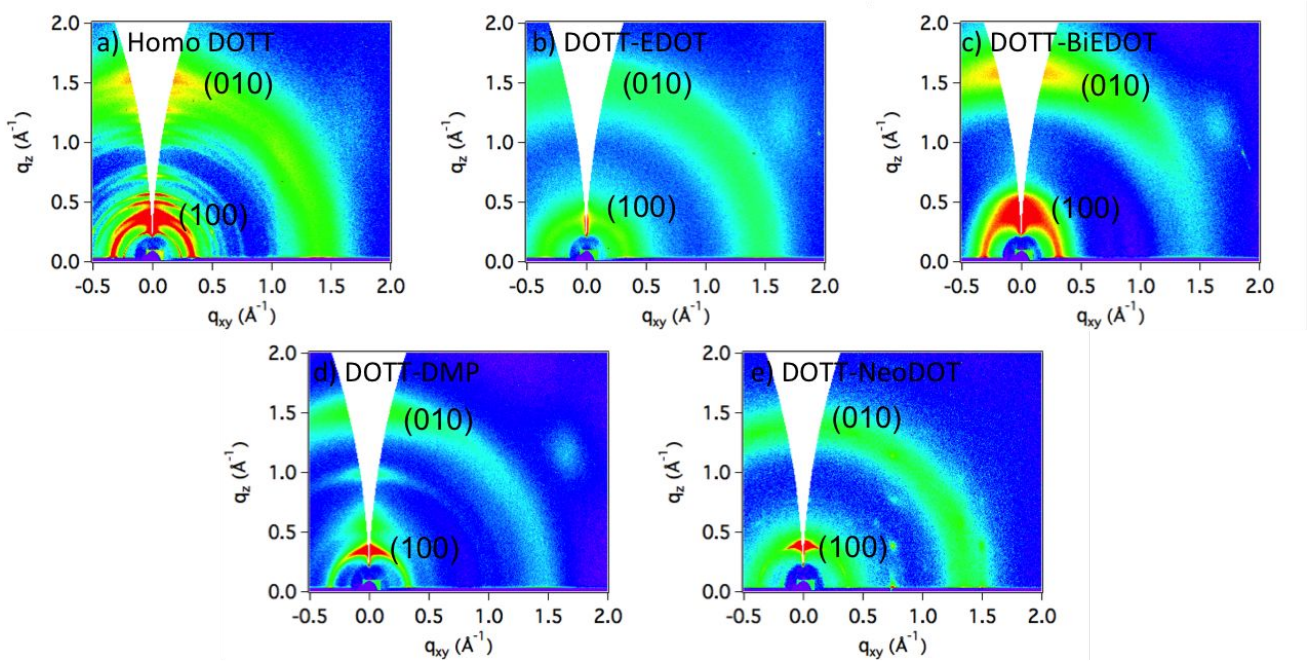

Figure 1: GIWAXS images of as-cast blade-coated films of Homo DOTT (a), DOTT-EDOT (b), DOTT-BiEDOT (c), DOTT-DMP (d), and DOTT-NeoDOT (e) on silicon wafers.

Homo DOTT, DOTT-EDOT, and DOTT-DMP, show the lamellar (100) diffraction band at Q_z = 0.34 Å^{-1} (interplanar distance d = 18 Å). The scattering images for DOTT-BiEDOT (Figure 1c) and DOTT NeoDOT (Figure 1e), show a slight shift towards tighter lamellar spacings (smaller q), of 17 Å and 16 Å respectively. Given the length of the side chains of these materials (10 carbon atoms), all of these spacing distances indicate lamellar interdigitation. In the case of the π-π stacking distances (010 plane), all of the polymers show diffraction bands at Q_z = 1.5 Å^{-1} (interplanar distance d = 4.2 Å), with the exception of DOTT-NeoDOT (Figure 1e), which shows a diffraction band at Q_z = 1.3 Å^{-1} (interplanar distance d = 4.8 Å). The spacing distances for the majority of the DOTT polymers are tighter than those found for branched and linear chain dioxythiophene homopolymers, which had interplanar distances of 4.5 Å.[48] DOTT-NeoDOT on the other hand has a larger π-π stacking distance by 0.3 Å than the dioxythiophene polymers. All of these dioxy-based thiophene and thienothiophene polymers have larger π-π stacking distances by about 1 Å as compared to P3HT for example, which is in the range of 3.7-3.8 Å.[14, 49-51] It is interesting to note that DOTT-NeoDOT has the smallest lamellar spacing distance and the largest π-π stacking distance. This trend is likely due to the steric bulk of the neopentyl groups (which are shorter in length than the hexyldecyl solubilizing side chains substituted onto the other polymers in the family) on the dioxythiophene. While this bulk does not increase the distance between the lamellae, it prevents the backbones of the polymer chains from coming close together. Despite the differences in the scattering patterns of these polymers, all materials, except Homo DOTT, show smooth and continuous films as evidenced by the atomic force microscopy (AFM) images, as seen in Figure S11, and photographs, as seen in Figure S12. The Homo DOTT polymer forms films that are rougher (Figure S11a) than

the other polymers in the family, as the AFM height image shows a height range that is 2.5 times larger than for the other images. Films of Homo DOTT are still continuous as evidenced by the photographs in Figure S12a. It is interesting to note that Homo DOTT has a high degree of intermolecular ordering and a significantly rougher film topography as compared to the other polymers in the family.

2.3 Chemical Oxidation and Solid-State Conductivity

It is not only important to understand how the polymer structure can affect overall morphology, but it is also important to understand how these properties relate to the processes of doping and overall electrical conductivity. In this study, all polymer films were chemically oxidized after film formation using solutions of chemical oxidants in propylene carbonate. Sequential doping was chosen as the doping method as it has been shown to disrupt the polymer microstructure to a lesser degree than co-processing the polymer and dopant.[49, 52-53] Propylene carbonate was selected as the solvent for the chemical oxidant solutions as it can dissolve the chemical oxidants, but not the polymer films and is the same solvent used for the electrochemical characterizations that will be discussed in the next section. Doping times of 30 seconds were selected because, upon further exposure to solutions of Magic Blue, polymer films showed delamination from the substrate. After exposure for 30 s, polymer films were rinsed with clean methanol in order to remove any excess dopant before further experimentation. Methanol was chosen as the rinsing solvent as it can dissolve both dopants chosen for this study (discussed below), propylene carbonate, and is a low boiling point solvent which allows doped films to dry faster than when rinsing with propylene carbonate. For this work, two dopants were selected in order to probe the structure-property relationships of the DOTT polymers and

chemical oxidants. These two dopants were Magic Blue and F4TCNQ. These dopants were selected as they are both considered to be strong electron acceptors,[54] with $E_{1/2}$ values above 0.2 V *vs*. Ag/Ag^+ as shown in Figure S13, but have drastically different structures after accepting an electron as shown in Figure S14. Here, Magic Blue has two components, both the electron-accepting triphenyl amine and the counterbalancing $SbCl_6$ anion, whereas the single F4TCNQ molecule acts as both the electron acceptor and counterbalancing anion to the charged polymer film.

As the optical properties of the polymers in the DOTT family depend on their redox state, we are able to track their extent of oxidation using UV-vis spectroscopy. In their neutral state, all of the polymers absorb in the visible region of the spectrum. Upon exposure to either 10 mM Magic Blue or F4TCNQ, all polymers are oxidized from their neutral form, and absorb in the infrared. Figure 2 shows example spectra corresponding to DOTT-EDOT (Figure 2a) and DOTT-NeoDOT (Figure 2b), and the spectra corresponding to the remaining polymers can be seen in Figure S15. The $SbCl_6$ anion in Magic Blue does not absorb light in the shown region of the spectrum, so there are not any additional contributions besides the oxidized polymer absorption when using this chemical oxidant. In contrast, F4TCNQ in its neutral and radical anion state (as shown in red) both absorb in the visible region of the spectrum.[55] The peak occurring around 400 nm corresponds to the neutral F4TCNQ molecule, and the peaks seen between 600-900 nm correspond to a mix of the polaronic charge carriers from the oxidized polymers as well as the F4TCNQ anion.

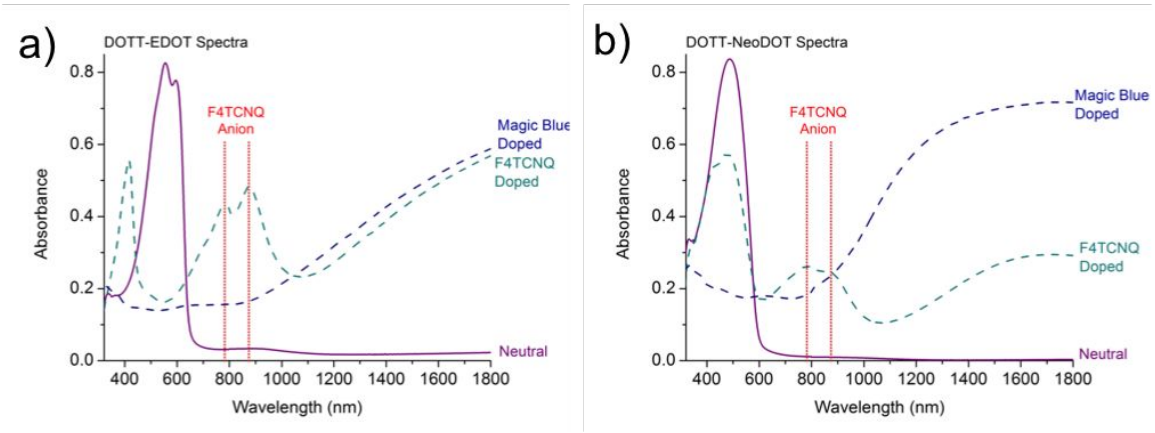

Figure 2: UV-vis absorption spectra of blade-coated polymer films of (a) DOTT-EDOT and (b) DOTT-NeoDOT on glass before and after 30 s of exposure to a 10 mM solution of either Magic Blue (dark blue curve) or F4TCNQ (dark cyan curve) in propylene carbonate and a methanol rinse.

When doping with both Magic Blue and F4TCNQ, it can be seen that the neutral π-π^* absorbance of DOTT-EDOT is fully depleted, while this absorbance is still observed when doping DOTT-NeoDOT with F4TCNQ. The neutral absorbance for Homo DOTT is also not fully depleted when doping with F4TCNQ (Figure S6a). It can be seen that both dopants result in the generation of polaronic charge carriers for Homo DOTT and DOTT-NeoDOT, as evidenced by their absorbance in the near infrared. The electrochemical properties of the polymer family will be discussed further on, but this difference in the extent of oxidation likely has to do with the differences in morphology of the polymer films. From the GIWAXS measurements of Homo DOTT and DOTT-NeoDOT (Figure 1a and 1e) we see that Homo DOTT is highly ordered and DOTT-NeoDOT has tighter lamellar spacing distances as compared to the other polymers. Work from Thomas *et al.* in 2018 showed that for a thiophene polymer with branched side chains, the steric bulk from the polymer sidechain can prevent effective charge transfer and complete doping when using F4TCNQ in vapor phase doping.[19] In this work, the authors concluded that due to

the bulk of the (2'-ethyl)hexyl side chain caused the molecular dopant to reside between the π-faces of the polymer crystallites, resulting in only partial charge transfer. Here, it is hypothesized that, because Homo DOTT is highly ordered and DOTT-NeoDOT possesses more steric bulk in its repeat unit, these polymers are more locked in conformation and have film morphologies that hinder charge transfer with F4TCNQ. In contrast, it is likely that the higher oxidation strength of the Magic Blue dopant allows it to more fully dope these more highly ordered polymers.

Turning to the more disordered polymer systems, the spectra corresponding to DOTT-BiEDOT (Figure S15b), and DOTT-DMP (Figure S15c), show that when doping with either Magic Blue or F4TCNQ a complete depletion of the neutral π-π^* transition and growth of absorbance between 900-1800 nm can also be observed. DOTT-BiEDOT is a unique polymer in the family, as it has an onset of oxidation that is sufficiently low enough to oxidize in air. The absorbance centered at 850 nm in the neutral curve of Figure S15b corresponds to polaronic charge carriers. As can be seen in Figure 2 and Figure S15, this is not present for any of the other polymers in the family.

In addition to understanding how the structure and morphology of the polymers can affect the extent of oxidation after exposure to chemical oxidants, it is also important to understand how this parameter can affect the overall electrical conductivity. Electrical conductivity is dependent on both the number of charge carriers and their mobility.[56] Furthermore, when considering chemically doped semiconducting polymers, it is important to understand that the polaron concentration and the charge carrier hopping mobility fluctuates significantly as a function of energetic and spatial coordinate.[17, 57] Electrical conductivity measurements as a function of dopant species and concentration

can provide guidance and reasoning for future electrical conductivity optimizations when used in conjunction with structural and spectral characterizations.

Figure 3 shows the electrical conductivity as a function of polymer repeat unit (Homo DOTT [HD], DOTT-EDOT [DE], DOTT-BiEDOT [DE_2], DOTT-DMP [DD], and DOTT-NeoDOT [DN]) and dopant species. In the pristine state (not doped), these polymers have electrical conductivities, as measured using the Van der Pauw technique, of less than 10^{-5} S/cm. Upon doping with 10 mM Magic Blue or F4TCNQ, all polymers in this study show at least a two order of magnitude increase in the electrical conductivity after chemical oxidation. The conductivity of DOTT-BiEDOT (DE_2) increases by 6 orders of magnitude and approaches 20 S/cm, which exceeds many values reported in the literature by up to two orders of magnitude for the commonly studied P3HT:F4TCNQ system using various chemical doping procedures including solution co-processing,[36, 50, 52, 58-60] and sequential doping.[14, 38, 49, 52]

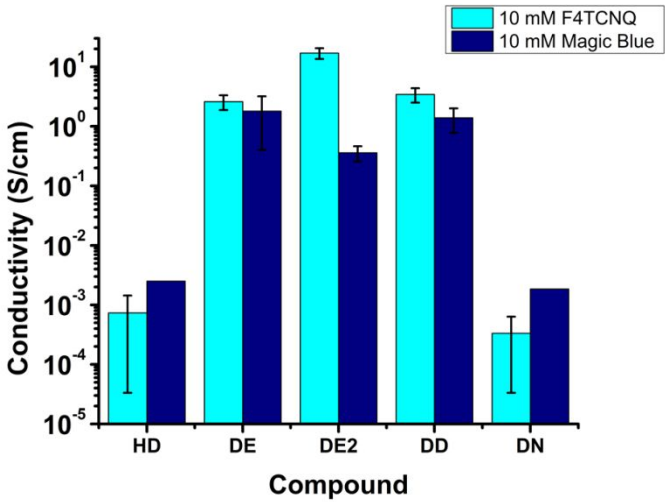

Figure 3: The electronic conductivity values of blade-coated polymer films on glass after exposure to either a 0.01 M Magic Blue or 10 mM M F4TCNQ solution in propylene carbonate for 30 seconds and a subsequent methanol rinse.

We observe that in general, DE, DE_2, and DD show the highest electrical conductivities by 3 orders of magnitude as compared to HD and DN when doping with either Magic Blue or F4TCNQ. Furthermore, we observe that as the dopant chemical species changes from Magic Blue to F4TCNQ, electrical conductivity generally increases (Figure 3). This observation is initially counterintuitive as Magic Blue has a higher oxidation potential than F4TCNQ and should generate more charge carriers (Figure S13). We observe at a 10 mM concentration that Magic Blue does indeed generate more charge carriers than F4TCNQ (Table S1 and Table S2), but we also observe that the microstructure is more heavily disrupted by Magic Blue than F4TCNQ given the larger lamellar and π-π spacing distances after chemical oxidation with Magic Blue as seen in Table S3. For example, we see that for Homo DOTT the lamellar spacing is 2.1 Å larger when doping with Magic Blue as compared to F4TCNQ. Turning to the π-π spacing distance of this polymer, the spacing is 1 Å larger when doping with Magic Blue. Turning to the DOTT-BiEDOT polymer, we see a 3.7 Å increase in the lamellar spacing when doping with Magic Blue as compared to F4TCNQ and a 0.6 Å increase in the π-π spacing distance. We hypothesize that doping with Magic Blue disrupts the microstructure to a greater extent than F4TCNQ because Magic Blue doping involves an octahedral $SbCl_6$ counterion while F4TCNQ doping yields a planar anion.[55] Recent studies have suggested that bulkier counterions likely disrupt the microstructure and decrease the polaron hopping mobility and electrical conductivity more than their planar counterparts,[61] and the $SbCl_6$ *vs.* F4TCNQ comparison herein further supports these previous studies.

Because of its higher electrical conductivity, F4TCNQ doping was further explored by varying the dopant concentration. Figure 4 shows the electrical conductivity as a function of F4TCNQ doping concentration (1 to 50 mM) and polymer repeat unit.

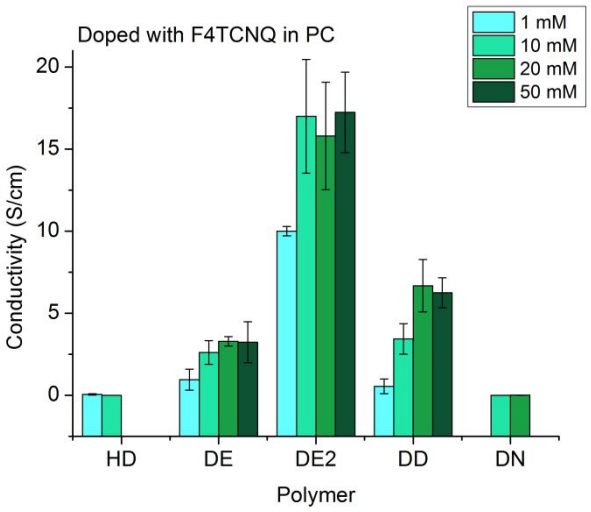

Figure 4: The electronic conductivity values of blade-coated polymer films on glass after exposure to F4TCNQ dopant solutions of varying concentrations in propylene carbonate for 30 seconds and a subsequent methanol rinse.

We note the electrical conductivity generally increases with increasing doping concentration. Interestingly, however, we observe that the electrical conductivity for DE, DE_2, and DD plateaus when excessively doped with chemical oxidants; oftentimes, the electrical conductivity decreases, which is attributed to increased carrier scattering or increased trap sites when excessively doped.[61-63] The electrical conductivity of DE, DE_2, and DD remain effectively invariant as doping increases from 20 to 50 mM (the measured values are within error bars). Based on XPS characterizations (Table S2), we observe that increasing F4TCNQ dopant concentration from 1 to 10 mM leads to increased charge carrier concentration, but increasing F4TCNQ dopant concentration from 10 to 50 mM does not appreciably increase the charge carrier concentration nor the electrical

conductivity. This implies that increased oxidant solution concentration does not necessarily lead to increased charge carrier creation nor necessitate deleterious structural effects. Based on this observation and implication, it is possible that F4TCNQ may not have the requisite oxidation strength to create additional charge carriers at higher solution concentrations, and that DE and DE_2 may permit a higher degrees of dopant infiltration without permanently disrupting the microstructure or improving the conductivity.[64-65] Additionally, we observe that electrical conductivity increases from DE to DD to DE_2 at 50 mM F4TCNQ. We can relate this trend to the increased degree of structural order and tighter π-π spacing distances demonstrated by DE_2 as compared to the other polymers after doping with F4TCNQ as seen in Figure S16. In addition to conductivity values approaching 20 S/cm, polymers in the DOTT family also demonstrate enhanced air stability in the doped state. Figure S17 shows the polymers' normalized retained conductivity as a function of the number of days oxidized films have been stored in ambient lab conditions. Measurements were taken for DE, DE_2, and DD films that were oxidized with solutions of F4TCNQ with concentrations ranging from 1-50 mM in propylene carbonate. As seen in Figure S17, the concentration of dopant has little effect on the overall retention of original conductivity, rather the degree of retention depends on the polymer structure. DE and DD have similar trends in that they lose up to 50% of their original conductivity, however, DE_2 retains over 70 % of its original conductivity after being stored in ambient conditions for 2 weeks. This is a significant increase in the doped air stability relative to polymers such as PBTTT, which in our experimentation was shown to lose all of its conductivity within 3 hours of doping.

2.4 Electrochemical Characterization

Considering the variety of applications for CPs, it is also important to understand how the structure of the DOTT family can affect their redox properties. In order to understand the electrochemical doping process of the DOTT polymers, films were drop-cast onto glassy carbon electrodes and studied using conventional voltammetry techniques. The onset of oxidation is probed by differential pulse voltammetry (DPV). Cyclic voltammetry (CV) is used to measure the ease at which an electron can be removed from the polymer film and the polymer film's current response as a function of applied potential. The DPV results can be seen in Figure S18, and the CVs of each polymer are shown in Figure 5.

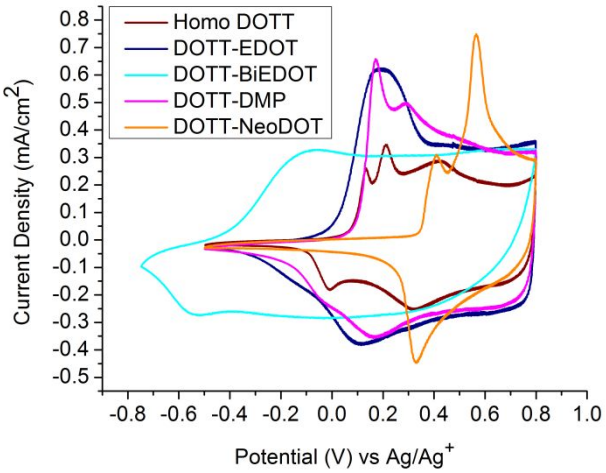

Figure 5: Cyclic voltammograms for drop-cast films of Homo DOTT in red, DOTT-EDOT in navy blue, DOTT-BiEDOT in cyan, DOTT-DMP in magenta, and DOTT-NeoDOT in orange on a glassy carbon electrode as the working electrode in a three-electrode cell in 0.5 M $TBAPF_6$ in propylene carbonate at a scan rate of 50 mV/s.

As with the morphology of the polymer films, we see that the polymer repeat unit structure has an effect on the onset of oxidation of the material. These onsets measured

through DPV cover a range of almost 0.9 V, with DOTT-BiEDOT being the easiest to oxidize at -0.62 V and DOTT-NeoDOT being the hardest to oxidize at 0.30 V. We see that with the addition of one EDOT moiety, the onset of oxidation is lowered by 0.14 V from 0.05 V for Homo DOTT, to -0.09 V for DOTT-EDOT. This onset is further lowered by 0.53 V the addition of a second EDOT unit for DOTT-BiEDOT. The onset of oxidation for DOTT-DMP occurs at -0.04 V. We see that the onsets of oxidation are within 0.1 V for Homo DOTT and DOTT-DMP and we would expect that when doping these two polymers they would generate a similar number of charges. We can see from the CV curve areas in Figure 5, that the relative area for DOTT-DMP is larger than for Homo DOTT, even though each electrode was carefully prepared by drop casting 4x 1 uL drops of a 1 mg/mL solution. Furthermore, from the XPS experiments (Table S2) we see that for a given concentration of F4TCNQ, fewer charge carriers are being generated for Homo DOTT as compared to the other polymers in the family. We hypothesize that the higher degrees of ordering observed for Homo DOTT is one reason why this polymer does not generate as many charge carriers as DOTT-DMP. The microstructure of Homo DOTT is significantly more perturbed (Table S3), with lamellar stacking distances increasing up to 5 Å after doping. This implies that it is more difficult for dopant and electrolyte ions to penetrate the polymer matrix in order to generate or stabilize any introduced charges.

As was discussed in the previous section, because the optical properties of these polymers are dependent on their redox state, we are able to monitor the polymer's doping level as a function of applied potential. Figure 6 shows the results for example spectroelectrochemical experiments for DOTT-EDOT (Figure 6a) and DOTT-NeoDOT (Figure 6b). The full spectroelectrochemical series for all polymers in the family

collectively can be seen in Figure S19. When increasing the potential from -0.5 to 0.8 V vs Ag/Ag^+ it can be seen that all polymers are fully oxidized, as evidenced through the complete depletion of their neutral π-π^* absorbance. Furthermore, upon the depletion of the neutral absorbance, we see a growth of absorbance beyond 700 nm for all materials. Here, the repeat unit of the polymer causes a difference in the number of intermediate states between the fully neutral polymer film (highlighted in red, at -0.5 V) and the fully oxidized polymer film (highlighted in blue, at 0.8 V). Homo DOTT (Figure S19a), DOTT-EDOT (Figure 6a), DOTT-BiEDOT (Figure S19c), and DOTT-DMP (Figure S19d) all have multiple intermediate states before the full depletion of their neutral absorbance, whereas DOTT-NeoDOT (Figure 6b), shows an almost immediate transition from the neutral to the fully oxidized state.

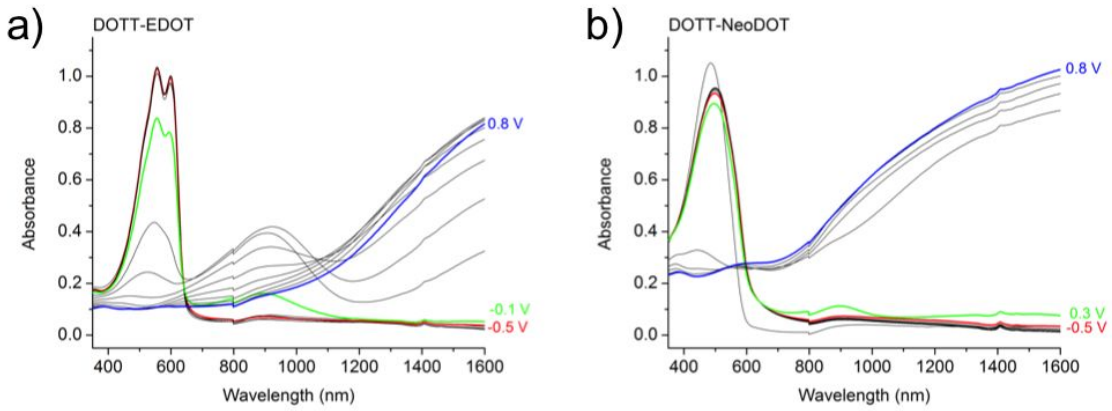

Figure 6: UV-vis absorption spectra as a function of applied potential of spray-coated polymer films of (a) DOTT-EDOT, and (e) DOTT-NeoDOT on ITO/glass in 0.5 M $TBAPF_6$ in propylene carbonate and conditioning cyclic voltammograms (f) with a scan rate of 50 mV/s.

In order to directly compare the trends for all the polymers, the results of these spectroelectrochemical experiments are shown collectively in Figure 7, where the

absorbance at λ_{max} for each polymer is plotted as a function of the applied potential. The extent of electrochemical doping follows the same trend as was seen with the extent of oxidation. The neutral π-π^* absorption for DOTT-BiEDOT begins to deplete at -0.6 V and the material is fully oxidized by 0.4 V. In contrast, the π-π^* absorption of DOTT-NeoDOT does not begin to deplete until 0.4 V, and no further evidence of optical changes are observed at higher potentials. The higher absorbances at potentials above 0.4 V for Homo DOTT and DOTT-NeoDOT, as compared to the other polymers in the family, are due to tailing of the oxidized state of these two materials into the visible region of the spectrum, as can be seen in Figures S19a (Homo DOTT) and S19e (DOTT-NeoDOT).

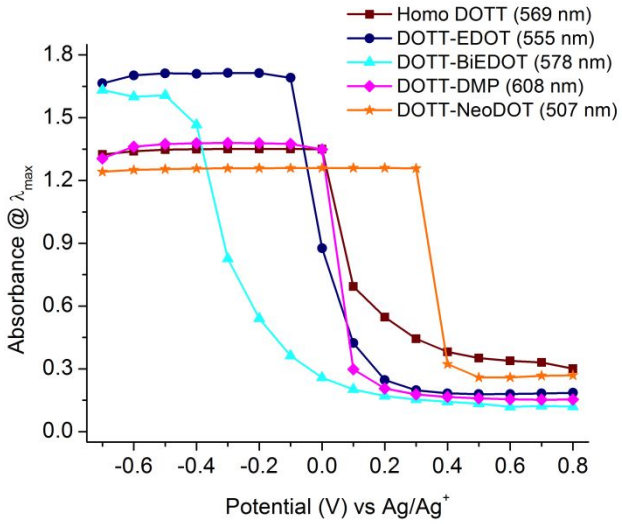

Figure 7: Absorbance values at each polymer's λ_{max} taken from UV-vis absorption spectra as a function of applied potential from -0.7 to 0.8 V versus Ag/Ag^+ for blade-coated Homo DOTT (red), DOTT-EDOT (navy blue), DOTT-BiEDOT (cyan), DOTT-DMP (magenta), and DOTT-NeoDOT (orange) films on ITO/glass in 0.5 M $TBAPF_6$ in propylene carbonate.

Turning to DOTT-DMP and Homo DOTT once again, it is interesting to note that it takes higher potentials to achieve the same degree of doping for Homo DOTT as compared to

DOTT-DMP. We see that more of the neutral π-π^* absorption peak is depleted at 0.1 V for DOTT-DMP as compared to that of Homo DOTT. Again, we observe evidence that it is harder for Homo DOTT to be doped as compared to DOTT-DMP, though they have the same onset of oxidation according to DPV. This is further support of the idea that the increased degree of intermolecular chain ordering inhibits both the electrochemical and chemical doping of the Homo DOTT polymer.

To further probe the effects of polymer structure on the redox processes of the DOTT polymer family, electrochemical conductance experiments were performed. Polymer films were drop-cast onto interdigitated microelectrodes, which were incorporated into an electrochemical cell.[66] The potential difference was held constant on one half of the microelectrodes, while the other half was cycled +/- 5 mV around the applied potential and the resulting current response was recorded. The potential window used for these experiments was -0.5 to 0.8 V vs an Ag/Ag^+ reference electrode and results were recorded at 0.1 V increments as shown in Figure 8. The conductance curve for each polymer was calculated from the average of three separate films. To confirm the reversibility of the polymer conductance, reverse direction curves (from high to low potential) can be seen in Figure S20, and a smaller conductance axis for polymers demonstrating low conductance values can be seen in Figure S21. The turn-on conductance response is observed to vary with the polymer onset of oxidation. DOTT-BiEDOT shows a turn-on at the lowest potential of -0.3 V, followed by DOTT-EDOT at 0.0 V, and DOTT-DMP at 0.1 V. All three of these polymers achieve high conductance values of around 6 mS at high potentials. As with the electrical conductivity data collected after chemical doping, the conductance of these materials does not drop back to 0 at the highest potential of 0.8 V. Similar to the

trends observed for the electrical conductivity data, we again see that Homo DOTT and DOTT-NeoDOT have the lowest conductance values overall. Homo DOTT does not demonstrate a conductance response until 0.2 V, and DOTT-NeoDOT turns on at 0.4 V (Figure S21). In comparison with the other polymers in the family, these materials have significantly lower overall conductance values. This experiment again highlights how polymer film morphology can affect charge transport.

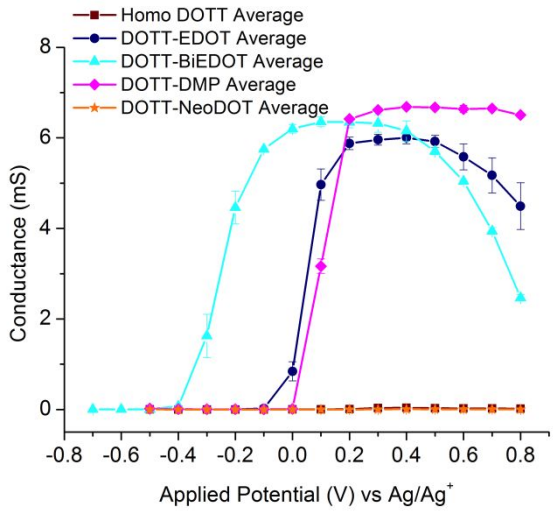

Figure 8: In situ conductance of Homo DOTT (red), DOTT-EDOT (navy blue), DOTT-BiEDOT (cyan), DOTT-DMP (magenta), and DOTT-NeoDOT (orange) from -0.5 to 0.8 V vs Ag/Ag^+ in 0.5 M $TBAPF_6$ in propylene carbonate. Averages taken from values collected from three films of each polymer.

Considering their similar onsets of oxidation, it would be expected that Homo DOTT and DOTT DMP would have similar turn-on values, however Homo DOTT requires a higher potential to give a conductance response. Similar to the electrical conductivity data, we also see that Homo DOTT is significantly less conductive than DOTT-DMP. Again, this is

likely due to the fact that the highly ordered microstructure of Homo DOTT is perturbed during doping, which leads to the inhibition of any charge transport processes.

3. Conclusions and Perspective:

The work presented in this study builds on the knowledge of how the polymer structure of DOTT-based conjugated polymers can relate to their charge transport properties. Soluble DOTT copolymers with EDOT linking units are shown to have conductivities that approach 20 S/cm after chemical doping with F4TCNQ and have electrochemical onsets of oxidation below 0 V *vs*. Ag/Ag^+. It was shown that materials with intermediate degrees of ordering had superior properties in that they had: higher electrical conductivities, lower onsets of oxidation, and higher electrochemical conductances as compared to the materials that had higher degrees of ordering. GIWAXS measurements showed that the polymers that demonstrated higher degrees of ordering had larger interchain spacing differences after the doping process, which resulted in solid-state conductivity values that were lower by orders of magnitude as compared to materials that demonstrated lower degrees of ordering. Comparing results for the polymers Homo DOTT and DOTT-DMP show that while polymers may have the same electrochemical ease of oxidation, they can have a three order of magnitude difference in their solid-state conductivity after chemical oxidation. The GIWAXS results for DOTT-DMP showed that this polymer had an intermediate degree of order as compared to Homo DOTT. After doping with F4TCNQ, the microstructure of this polymer film was not disrupted, which implied that the molecular dopant was able to interact with the polymer matrix such that charge transfer could occur and the newly generated charges could be effectively delocalized without being trapped. We find that highly ordered polymer films are more

difficult to oxidize through both chemical and electrochemical processes and transport charge as compared to less ordered polymer systems. It was hypothesized that highly ordered polymer systems have a more "locked conformation" which prevents the ease of oxidation and delocalization of charge along the backbone.

Furthermore, when selecting dopants for high electrical conductivity applications, the strength of the dopant is not the sole determinant in the overall electrical conductivity value. Results showed that it is important to understand the geometric interactions between the polymer film and chemical oxidant, which is a concept that has been shown in other work reported in the literature.[19] Even though Magic Blue had a sufficient oxidizing strength, its bulky structure caused the microstructure of the polymer films to be more perturbed than when doping with F4TCNQ. A combination of GIWAXS, XPS, UV-Vis absorption, and in-plane solid-state conductivity measurements showed that the two chemical oxidants could generate charge carriers in polymers that were highly ordered, but a combination of the disruptions of the microstructure of the polymer films and bulkiness of the substituents on the polymer backbone prevented high conductivities from being attained. This unique family of polymers has demonstrated the multiple factors that can inhibit both chemical and electrochemical oxidation and transport of charge.

5. Experimental Section:

5.1 Film Formation

The synthesis and structural confirmation for the polymers used in this study was performed as described in the supporting information. The Poly[2,5-bis(3-hexadecylthiophen-2-yl)thieno[3,2-b]thiophene] (PBTTT-C16) sample used for comparison for air stability measurements was purchased from Luminescence Technology Corporation (LT-S9060 PBTTT-C16, MW = > 40,000) and was used without further purification. Before film formation, 30-40 mg mL^{-1} polymer samples were prepared in chloroform. Films were blade-coated onto either glass substrates or ITO-glass substrates (25 mm x 75 mm x 0.7 mm, sheet resistance 8-12 Ω sq^{-1}, Delta Technologies, Ltd) that were pre-rinsed and sonicated in solutions of sodium dodecyl sulfate-water, water, acetone, and finally isopropanol, and allowed to air dry. Once dry, polymer films were blade-coated with a custom blade-coater built in-house with a gap height of 100 μm and various coating speeds depending on solution viscosity. Films of each polymer were cast to a pre-determined optical density of 0.95 ± 0.1 at λ_{max} (552 nm for Homo DOTT, 555 nm for DOTT-EDOT, 566 nm for DOTT-BiEDOT, 588 nm for DOTT-DMP, and 492 nm for DOTT-NeoDOT). The spectroscopic properties of all films cast in this study were monitored with an Ocean Optics USB2000+ spectrophotometer detector using an Ocean Optics DH-2000-BAL fiber-optic light source.

5.2 Characterization of Intermolecular Ordering

AFM measurements were performed using a Bruker atomic force microscope (Dimension icon) with a Bruker Tap 150 cantilever (Model: RTESP-150) in standard tapping mode. Samples were prepared as described above on glass.

GIWAXS measurements were conducted at the Stanford Synchrotron Radiation Lightsource on beamline 11-3. Samples were prepared as described above on Si wafers that were washed using the same procedure as the glass substrates. Samples were irradiated with X-ray energy of 12.7 keV and their GIWAXS patterns were recorded with a 2-D image detector (MAR345 image plate detector). Typical exposure times were 180 s. The distance between the sample and the detector was kept at 250 mm and the incident angle was maintained at 0.13° in order to achieve the highest scattering intensity from the sample without interference from the substrate (polymer critical angle ~0.08°). The scattering images were calibrated using a LaB_6 standard. Samples were loaded into a chamber and purged with helium to reduce damage to the sample and reduce the air scattering background. The data analysis was conducted using the Nika software package for Wavemetrics Igor, in combination with WAXStools.[67-68] The images presented in this work are considered to be reproducible as multiple samples of the same polymer and doping condition were run and showed the same diffraction patterns.

5.3 Electrochemical Characterization

For all electrochemical characterizations the electrolyte solution was 0.5 M tetrabutylammonium hexafluorophosphate ($TBAPF_6$, Acros Organics, 98% and recrystallized using 200 mL of ethanol for every 100 g of salt) dissolved in propylene carbonate. A platinum flag served as the counter electrode and an Ag/Ag^+ electrode (10 mM $AgNO_3$ and 0.5 M $TBAPF_6$ in acetonitrile, +0.085 V vs Fc/Fc^+) was used as the reference electrode. The redox response of the films was characterized using DPV (step size 2 mV and step time 0.1 s) and CV (scan rate 50 mV/s) performed in a three-electrode cell, using a Princeton Applied Research 273 potentiostat/galvanostat under CorrWare

control and *in situ* conductance measurements were performed in a four-electrode cell using a Pine bipotentiostat (model AFCBP1) under control of Aftermath.

For electrochemical characterizations including differential pulse voltammetry (DPV), cyclic voltammetry (CV), four 1μL drops of polymer solutions with concentrations of 1 mg mL^{-1} were sequentially dropped onto polished glassy carbon electrodes and allowed to air dry. For the *in situ* conductance measurements, three 0.5 μL drops of polymer solutions with concentrations of 1 mg mL^{-1} were sequentially dropped onto Pt interdigitated microelectrodes (Abtech Scientific Inc. IME 1050.5 series) with 50 digits, 10 μm in width, and 10 μm separation and allowed to air dry.

For *in situ* conductance measurements on the interdigitated electrodes, one of the working electrodes was held at a given potential E (range from -0.5 to 0.8 V vs Ag/Ag^{+}) while cycling the second working electrode E ± 0.005 V at 0.5 mVs^{-1}. The slope of the resulting current density versus potential curve was used to determine the film conductance. Films were formed by drop-casting three 0.5 μL drops from 1mg/mL solutions.

Spectroelectrochemistry (and UV-Vis) measurements were performed in coordination with an Agilent Technologies Cary 5000 UV-Vis-NIR Spectrophotometer under Cary WinUV control. Corresponding photographs of the electrochemical cells used in these experiments were taken in a lightbooth that was illuminated by a D50 (5000K) lamp, using a Nikon D90 SLR camera with a Nikon 18-105 mm VR lens and are reported without further manipulation beyond photograph cropping.

5.4 Chemical Oxidation of Polymer Films

After casting, polymer films were exposed to dopant solutions made from propylene carbonate (99.5%, Acros Organics, purified using a solvent purification system from Vacuum Atmospheres) and varying concentrations of the dopant. The dopants used for this study, tris(4-bromophenyl)ammoniumyl hexachloroantimonate (Sigma Aldrich, technical grade), is here referred to as "Magic Blue", and Tetrafluorotetracyanoquinodimethane (TCI America, purified by sublimation), is here referred to as "F4TCNQ". Dopant solutions were prepared in an argon-filled glovebox in the case of Magic Blue and in air in the case of F4TCNQ. To perform chemical oxidation, dopant solutions with varying concentrations were drop-cast onto polymer films for 30 seconds. Subsequently, each film was rinsed with clean methanol. When preparing samples for atomic force microscopy (AFM), grazing-incidence wide-angle x-ray scattering (GIWAXS), and solid-state conductivity measurements, polymer films were dried under full vacuum at 50°C for 15 hours in a vacuum oven to ensure full removal of solvent.

5.5 XPS of Oxidized Polymer Films

XPS spectra were recorded using a Thermo Fisher K-Alpha Photoelectron Spectrophotometer, with a monochromatic Al K-α source (energy 1487 eV) and a hemispherical 180° detector. Samples were positioned with the electron takeoff angle normal to the surface of the sample, with respect to the analyzer. In all spectra, a low energy electron "flood gun" was used to maintain sample charge neutrality during the measurement. Spectra were recorded for the S 2p, C 1s, F 1s, and Cl 2p core levels using a pass energy of 50 eV, with a spot size of 400 μm. Curve fitting and elemental composition

calculations were carried out on the high-resolution elemental spectrum of each sample, using the curve-fit feature of the XPS analysis software CasaXPS. Doping ratios were calculated from the atomic abundance values of each element which were calculated according to eq 1: $atomic\ abundance = \frac{A_{rel}}{RSF * KE^{0.6}}$ where A_{rel} is the integrated area for the fits of each peak in the elemental high-resolution spectra, RSF is the relative sensitivity factor for each element, and KE is the kinetic energy. Example plots of fitted XPS data can be seen in Figure S22.

5.6 Solid-state Conductivity and Thermoelectric Measurements

Four gold contact pads (1 mm × 1 mm, ~ 100 nm thick) were deposited on doped films using a shadow mask and a home-built DC sputtering chamber. Contact pad and film thicknesses were measured using a Profilm 3D optical profilometer. Initial electrical conductivity and Seebeck measurements were made on a custom setup[69-70] on the same day as contact pad deposition. Micromanipulators with tungsten tips were used to make electrical contact to the gold contact pads and in-plane electrical conductivity was acquired using the four-probe Van der Pauw technique. The Seebeck coefficient was measured by suspending the sample between two temperature-controlled Peltier units (separated ~3 mm) and applying a series of temperature differences up to ΔT=10 K between the stages. The thermoelectric voltage was measured between two contact pads on separate stages using the probe tips, while the temperature of each pad was measured with a K-type thermocouple near the probe tips. Voltage and temperature data were acquired using a Keithley 2700 DMM with a 7708 Mux card via a LabVIEW interface. The Seebeck coefficient was extracted as the slope of the *V vs.* ΔT plot. All measurements were made in ambient atmosphere and lighting.

Author Contributions:

J.F.P. synthesized and confirmed the structure of all of the polymers studied in this work. S.A.G. carried out and analyzed the solid-state conductivity measurements. S.L.P. carried the planning, execution, and evaluation of all other experimentation corresponding to the redox and solid-state measurements. S.Y. and J.R. assisted with the interpretation of the data. All authors contributed to writing this manuscript and have given approval of the final version.

Funding:

The authors appreciate the support of the Office of Naval Research (Grant Number N00014-18-1-2222) for funding. S.A.G. appreciates the support of the Office of Naval Research (award number N00014-19-1-2162), Department of Education Graduate Assistance in Areas of National Need (GAANN) program at the Georgia Institute of Technology (Award #P200A180075), Link Energy Foundation, and the Science and Technology of Material Interfaces (STAMI) group at the Georgia Institute of Technology.

Notes:

The authors declare the following competing financial interest (s): Electrochromic polymer technology developed at the University of Florida and the Georgia Institute of Technology has been licensed to NXN Licensing. J.R.R. serves as a consultant to NXN Licensing.

Acknowledgements:

Part of this work was performed in part at the Georgia Tech Institute for Electronics and Nanotechnology, a member of the National Nanotechnology Coordinated Infrastructure, which is supported by the National Science Foundation (Grant ECCS-1542174). The

authors gratefully acknowledge Maged Abdelsami in the group of Dr. Michael Toney at Stanford for assistance with the GIWAXS data interpretation. In addition, thank you to D. Eric Shen for advice and assistance with data analysis discussion and interpretation. Finally, we would like to thank Brandon DiTullio for performing Gel Permeation Chromatography experiments to measure molecular weights and distributions of the polymers in this study. We acknowledge support from Science and Technology of Material Interfaces (STAMI) at Georgia Tech for use of the shared characterization facility.

REFERENCES

1. Chung, D. D. L., Materials for Electromagnetic Interference Shielding. *Journal of Materials Engineering and Performance* **2000,** *9* (3), 350-354.
2. Dhawan, S. K.; Singh, N.; Venkatachalam, S., Shielding behaviour of conducting polymer-coated fabrics in X-band, W-band and radio frequency range. *Synthetic Metals* **2002,** *129* (3), 261-267.
3. Kroon, R.; Mengistie, D. A.; Kiefer, D.; Hynynen, J.; Ryan, J. D.; Yu, L.; Müller, C., Thermoelectric plastics: from design to synthesis, processing and structure–property relationships. *Chemical Society Reviews* **2016,** *45* (22), 6147-6164.
4. Russ, B.; Glaudell, A.; Urban, J. J.; Chabinyc, M. L.; Segalman, R. A., Organic thermoelectric materials for energy harvesting and temperature control. *Nature Reviews Materials* **2016,** *1*, 16050.
5. Chiang, C. K.; Fincher, C. R.; Park, Y. W.; Heeger, A. J.; Shirakawa, H.; Louis, E. J.; Gau, S. C.; MacDiarmid, A. G., Electrical Conductivity in Doped Polyacetylene. *Physical Review Letters* **1977,** *39* (17), 1098-1101.
6. Shirakawa, H.; Louis, E. J.; MacDiarmid, A. G.; Chiang, C. K.; Heeger, A. J., Synthesis of electrically conducting organic polymers: halogen derivatives of polyacetylene, (CH). *Journal of the Chemical Society, Chemical Communications* **1977,** (16), 578-580.
7. Kim, Y. H.; Sachse, C.; Machala, M. L.; May, C.; Müller-Meskamp, L.; Leo, K., Highly Conductive PEDOT:PSS Electrode with Optimized Solvent and Thermal Post-Treatment for ITO-Free Organic Solar Cells. *Advanced Functional Materials* **2011,** *21* (6), 1076-1081.
8. Jensen, J.; Hösel, M.; Dyer, A. L.; Krebs, F. C., Development and Manufacture of Polymer-Based Electrochromic Devices. *Advanced Functional Materials* **2015,** *25* (14), 2073-2090.
9. Mortimer, R. J.; Dyer, A. L.; Reynolds, J. R., Electrochromic organic and polymeric materials for display applications. *Displays* **2006,** *27* (1), 2-18.
10. Liu, D. Y.; Reynolds, J. R., Dioxythiophene-Based Polymer Electrodes for Supercapacitor Modules. *ACS Applied Materials & Interfaces* **2010,** *2* (12), 3586-3593.
11. Österholm, A. M.; Ponder, J. F.; Kerszulis, J. A.; Reynolds, J. R., Solution Processed PEDOT Analogues in Electrochemical Supercapacitors. *ACS Applied Materials & Interfaces* **2016,** *8* (21), 13492-13498.
12. Flagg, L. Q.; Bischak, C. G.; Onorato, J. W.; Rashid, R. B.; Luscombe, C. K.; Ginger, D. S., Polymer Crystallinity Controls Water Uptake in Glycol Side-Chain Polymer Organic Electrochemical Transistors. *Journal of the American Chemical Society* **2019,** *141* (10), 4345-4354.
13. Inal, S.; Rivnay, J.; Hofmann, A. I.; Uguz, I.; Mumtaz, M.; Katsigiannopoulos, D.; Brochon, C.; Cloutet, E.; Hadziioannou, G.; Malliaras, G. G., Organic electrochemical transistors based on PEDOT with different anionic polyelectrolyte dopants. *Journal of Polymer Science Part B: Polymer Physics* **2016,** *54* (2), 147-151.
14. Hynynen, J.; Kiefer, D.; Yu, L.; Kroon, R.; Munir, R.; Amassian, A.; Kemerink, M.; Müller, C., Enhanced Electrical Conductivity of Molecularly p-Doped Poly(3-

hexylthiophene) through Understanding the Correlation with Solid-State Order. *Macromolecules* **2017,** *50* (20), 8140-8148.
15. Scholes, D. T.; Yee, P. Y.; Lindemuth, J. R.; Kang, H.; Onorato, J.; Ghosh, R.; Luscombe, C. K.; Spano, F. C.; Tolbert, S. H.; Schwartz, B. J., The Effects of Crystallinity on Charge Transport and the Structure of Sequentially Processed F4TCNQ-Doped Conjugated Polymer Films. *Advanced Functional Materials* **2017,** *27* (44), 1702654.
16. Yee, P. Y.; Scholes, D. T.; Schwartz, B. J.; Tolbert, S. H., Dopant-Induced Ordering of Amorphous Regions in Regiorandom P3HT. *The Journal of Physical Chemistry Letters* **2019**, 4929-4934.
17. Noriega, R.; Rivnay, J.; Vandewal, K.; Koch, F. P. V.; Stingelin, N.; Smith, P.; Toney, M. F.; Salleo, A., A general relationship between disorder, aggregation and charge transport in conjugated polymers. *Nature Materials* **2013,** *12*, 1038.
18. Dong, B. X.; Nowak, C.; Onorato, J. W.; Strzalka, J.; Escobedo, F. A.; Luscombe, C. K.; Nealey, P. F.; Patel, S. N., Influence of Side-Chain Chemistry on Structure and Ionic Conduction Characteristics of Polythiophene Derivatives: A Computational and Experimental Study. *Chemistry of Materials* **2019,** *31* (4), 1418-1429.
19. Thomas, E. M.; Davidson, E. C.; Katsumata, R.; Segalman, R. A.; Chabinyc, M. L., Branched Side Chains Govern Counterion Position and Doping Mechanism in Conjugated Polythiophenes. *ACS Macro Letters* **2018,** *7* (12), 1492-1497.
20. Liang, Z.; Zhang, Y.; Souri, M.; Luo, X.; Boehm, Alex M.; Li, R.; Zhang, Y.; Wang, T.; Kim, D.-Y.; Mei, J.; Marder, S. R.; Graham, K. R., Influence of dopant size and electron affinity on the electrical conductivity and thermoelectric properties of a series of conjugated polymers. *Journal of Materials Chemistry A* **2018,** *6* (34), 16495-16505.
21. Scholes, D. T.; Yee, P. Y.; McKeown, G. R.; Li, S.; Kang, H.; Lindemuth, J. R.; Xia, X.; King, S. C.; Seferos, D. S.; Tolbert, S. H.; Schwartz, B. J., Designing Conjugated Polymers for Molecular Doping: The Roles of Crystallinity, Swelling, and Conductivity in Sequentially-Doped Selenophene-Based Copolymers. *Chemistry of Materials* **2019,** *31* (1), 73-82.
22. Dietrich, M.; Heinze, J.; Heywang, G.; Jonas, F., Electrochemical and spectroscopic characterization of polyalkylenedioxythiophenes. *Journal of Electroanalytical Chemistry* **1994,** *369* (1), 87-92.
23. Heinze, J.; Frontana-Uribe, B. A.; Ludwigs, S., Electrochemistry of Conducting Polymers—Persistent Models and New Concepts. *Chemical Reviews* **2010,** *110* (8), 4724-4771.
24. Österholm, A. M.; Ponder, J. F.; De Keersmaecker, M.; Shen, D. E.; Reynolds, J. R., Disentangling Redox Properties and Capacitance in Solution-Processed Conjugated Polymers. *Chemistry of Materials* **2019**.
25. Giovannitti, A.; Sbircea, D.-T.; Inal, S.; Nielsen, C. B.; Bandiello, E.; Hanifi, D. A.; Sessolo, M.; Malliaras, G. G.; McCulloch, I.; Rivnay, J., Controlling the mode of operation of organic transistors through side-chain engineering. *Proceedings of the National Academy of Sciences* **2016,** *113* (43), 12017-12022.
26. Inal, S.; Rivnay, J.; Leleux, P.; Ferro, M.; Ramuz, M.; Brendel, J. C.; Schmidt, M. M.; Thelakkat, M.; Malliaras, G. G., A High Transconductance Accumulation Mode Electrochemical Transistor. *Advanced Materials* **2014,** *26* (44), 7450-7455.

27. Rivnay, J.; Owens, R. M.; Malliaras, G. G., The Rise of Organic Bioelectronics. *Chemistry of Materials* **2014,** *26* (1), 679-685.
28. Rivnay, J.; Inal, S.; Salleo, A.; Owens, R. M.; Berggren, M.; Malliaras, G. G., Organic electrochemical transistors. *Nature Reviews Materials* **2018,** *3*, 17086.
29. Nielsen, C. B.; Giovannitti, A.; Sbircea, D.-T.; Bandiello, E.; Niazi, M. R.; Hanifi, D. A.; Sessolo, M.; Amassian, A.; Malliaras, G. G.; Rivnay, J.; McCulloch, I., Molecular Design of Semiconducting Polymers for High-Performance Organic Electrochemical Transistors. *Journal of the American Chemical Society* **2016,** *138* (32), 10252-10259.
30. Ponder Jr., J. F.; Menon, A. K.; Dasari, R. R.; Pittelli, S. L.; Thorley, K. J.; Yee, S. K.; Marder, S. R.; Reynolds, J. R., Conductive, Solution-Processed Dioxythiophene Copolymers for Thermoelectric and Transparent Electrode Applications. *Advanced Energy Materials* **2019,** *9* (24), 1900395.
31. Cirpan, A.; Argun, A. A.; Grenier, C. R. G.; Reeves, B. D.; Reynolds, J. R., Electrochromic devices based on soluble and processable dioxythiophene polymers. *Journal of Materials Chemistry* **2003,** *13* (10), 2422-2428.
32. Savagian, L. R.; Österholm, A. M.; Ponder Jr., J. F.; Barth, K. J.; Rivnay, J.; Reynolds, J. R., Balancing Charge Storage and Mobility in an Oligo(Ether) Functionalized Dioxythiophene Copolymer for Organic- and Aqueous- Based Electrochemical Devices and Transistors. *Advanced Materials* **2018,** *30* (50), 1804647.
33. Jow, T. R.; Jen, K. Y.; Elsenbaumer, R. L.; Shacklette, L. W.; Angelopoulos, M.; Cava, M. P., Electrochemical studies of fused-thiophene systems. *Synthetic Metals* **1986,** *14* (1), 53-60.
34. Patel, S. N.; Glaudell, A. M.; Peterson, K. A.; Thomas, E. M.; O'Hara, K. A.; Lim, E.; Chabinyc, M. L., Morphology controls the thermoelectric power factor of a doped semiconducting polymer. *Science Advances* **2017,** *3* (6).
35. Karpov, Y.; Erdmann, T.; Raguzin, I.; Al-Hussein, M.; Binner, M.; Lappan, U.; Stamm, M.; Gerasimov, K. L.; Beryozkina, T.; Bakulev, V.; Anokhin, D. V.; Ivanov, D. A.; Günther, F.; Gemming, S.; Seifert, G.; Voit, B.; Di Pietro, R.; Kiriy, A., High Conductivity in Molecularly p-Doped Diketopyrrolopyrrole-Based Polymer: The Impact of a High Dopant Strength and Good Structural Order. *Advanced Materials* **2016,** *28* (28), 6003-6010.
36. Glaudell, A. M.; Cochran, J. E.; Patel, S. N.; Chabinyc, M. L., Impact of the Doping Method on Conductivity and Thermopower in Semiconducting Polythiophenes. *Advanced Energy Materials* **2015,** *5* (4), 1401072.
37. Vijayakumar, V.; Zhong, Y.; Untilova, V.; Bahri, M.; Herrmann, L.; Biniek, L.; Leclerc, N.; Brinkmann, M., Bringing Conducting Polymers to High Order: Toward Conductivities beyond 105 S cm−1 and Thermoelectric Power Factors of 2 mW m−1 K−2. *Advanced Energy Materials* **2019,** *9* (24), 1900266.
38. Hamidi-Sakr, A.; Biniek, L.; Bantignies, J.-L.; Maurin, D.; Herrmann, L.; Leclerc, N.; Lévêque, P.; Vijayakumar, V.; Zimmermann, N.; Brinkmann, M., A Versatile Method to Fabricate Highly In-Plane Aligned Conducting Polymer Films with Anisotropic Charge Transport and Thermoelectric Properties: The Key Role of Alkyl Side Chain Layers on the Doping Mechanism. *Advanced Functional Materials* **2017,** *27* (25), 1700173.

39. Weller, T.; Rundel, K.; Krauss, G.; McNeill, C. R.; Thelakkat, M., Highly Efficient and Balanced Charge Transport in Thieno[3,4-c]pyrrole-4,6-dione Copolymers: Dramatic Influence of Thieno[3,2-b]thiophene Comonomer on Alignment and Charge Transport. *The Journal of Physical Chemistry C* **2018,** *122* (14), 7565-7574.
40. Vijayakumar, V.; Zaborova, E.; Biniek, L.; Zeng, H.; Herrmann, L.; Carvalho, A.; Boyron, O.; Leclerc, N.; Brinkmann, M., Effect of Alkyl Side Chain Length on Doping Kinetics, Thermopower, and Charge Transport Properties in Highly Oriented F4TCNQ-Doped PBTTT Films. *ACS Applied Materials & Interfaces* **2019,** *11* (5), 4942-4953.
41. Kiefer, D. Molecular Doping of Polar Conjugated Polymers. Chalmers University of Technology, Sweden, 2019.
42. Cochran, J. E.; Junk, M. J. N.; Glaudell, A. M.; Miller, P. L.; Cowart, J. S.; Toney, M. F.; Hawker, C. J.; Chmelka, B. F.; Chabinyc, M. L., Molecular Interactions and Ordering in Electrically Doped Polymers: Blends of PBTTT and F4TCNQ. *Macromolecules* **2014,** *47* (19), 6836-6846.
43. Turbiez, M.; Frère, P.; Leriche, P.; Mercier, N.; Roncali, J., Poly(3,6-dimethoxy-thieno[3,2-b]thiophene): a possible alternative to poly(3,4-ethylenedioxythiophene) (PEDOT). *Chemical Communications* **2005,** (9), 1161-1163.
44. Li, W.; Guo, Y.; Shi, J.; Yu, H.; Meng, H., Solution-Processable Neutral Green Electrochromic Polymer Containing Thieno[3,2-b]thiophene Derivative as Unconventional Donor Units. *Macromolecules* **2016,** *49* (19), 7211-7219.
45. Yin, Y.; Li, W.; Zeng, X.; Xu, P.; Murtaza, I.; Guo, Y.; Liu, Y.; Li, T.; Cao, J.; He, Y.; Meng, H., Design Strategy for Efficient Solution-Processable Red Electrochromic Polymers Based on Unconventional 3,6-Bis(dodecyloxy)thieno[3,2-b]thiophene Building Blocks. *Macromolecules* **2018,** *51* (19), 7853-7862.
46. Guo, Y.; Li, W.; Yu, H.; Perepichka, D. F.; Meng, H., Flexible Asymmetric Supercapacitors via Spray Coating of a New Electrochromic Donor–Acceptor Polymer. *Advanced Energy Materials* **2017,** *7* (2), 1601623.
47. Alberga, D.; Perrier, A.; Ciofini, I.; Mangiatordi, G. F.; Lattanzi, G.; Adamo, C., Morphological and charge transport properties of amorphous and crystalline P3HT and PBTTT: insights from theory. *Physical Chemistry Chemical Physics* **2015,** *17* (28), 18742-18750.
48. Pittelli, S. L.; De Keersmaecker, M.; Ponder Jr, J. F.; Österholm, A. M.; Ochieng, M. A.; Reynolds, J. R., Structural effects on the charge transport properties of chemically and electrochemically doped dioxythiophene polymers. *Journal of Materials Chemistry C* **2020,** *8* (2), 683-693.
49. Scholes, D. T.; Hawks, S. A.; Yee, P. Y.; Wu, H.; Lindemuth, J. R.; Tolbert, S. H.; Schwartz, B. J., Overcoming Film Quality Issues for Conjugated Polymers Doped with F4TCNQ by Solution Sequential Processing: Hall Effect, Structural, and Optical Measurements. *The Journal of Physical Chemistry Letters* **2015,** *6* (23), 4786-4793.
50. Duong, D. T.; Wang, C.; Antono, E.; Toney, M. F.; Salleo, A., The chemical and structural origin of efficient p-type doping in P3HT. *Organic Electronics* **2013,** *14* (5), 1330-1336.
51. Méndez, H.; Heimel, G.; Winkler, S.; Frisch, J.; Opitz, A.; Sauer, K.; Wegner, B.; Oehzelt, M.; Röthel, C.; Duhm, S.; Többens, D.; Koch, N.; Salzmann, I., Charge-transfer crystallites as molecular electrical dopants. *Nature Communications* **2015,** *6*, 8560.

52. Jacobs, I. E.; Aasen, E. W.; Oliveira, J. L.; Fonseca, T. N.; Roehling, J. D.; Li, J.; Zhang, G.; Augustine, M. P.; Mascal, M.; Moulé, A. J., Comparison of solution-mixed and sequentially processed P3HT:F4TCNQ films: effect of doping-induced aggregation on film morphology. *Journal of Materials Chemistry C* **2016,** *4* (16), 3454-3466.
53. Jacobs, I. E.; Moulé, A. J., Controlling Molecular Doping in Organic Semiconductors. *Advanced Materials* **2017,** *29* (42), 1703063.
54. Connelly, N. G.; Geiger, W. E., Chemical Redox Agents for Organometallic Chemistry. *Chemical Reviews* **1996,** *96* (2), 877-910.
55. Kiefer, D.; Kroon, R.; Hofmann, A. I.; Sun, H.; Liu, X.; Giovannitti, A.; Stegerer, D.; Cano, A.; Hynynen, J.; Yu, L.; Zhang, Y.; Nai, D.; Harrelson, T. F.; Sommer, M.; Moulé, A. J.; Kemerink, M.; Marder, S. R.; McCulloch, I.; Fahlman, M.; Fabiano, S.; Müller, C., Double doping of conjugated polymers with monomer molecular dopants. *Nature Materials* **2019,** *18* (2), 149-155.
56. Bubnova, O.; Crispin, X., Towards polymer-based organic thermoelectric generators. *Energy & Environmental Science* **2012,** *5* (11), 9345-9362.
57. Kang, S. D.; Snyder, G. J., Charge-transport model for conducting polymers. *Nature Materials* **2016,** *16*, 252.
58. Yim, K.-H.; Whiting, G. L.; Murphy, C. E.; Halls, J. J. M.; Burroughes, J. H.; Friend, R. H.; Kim, J.-S., Controlling Electrical Properties of Conjugated Polymers via a Solution-Based p-Type Doping. *Advanced Materials* **2008,** *20* (17), 3319-3324.
59. Kiefer, D.; Yu, L.; Fransson, E.; Gómez, A.; Primetzhofer, D.; Amassian, A.; Campoy-Quiles, M.; Müller, C., A Solution-Doped Polymer Semiconductor:Insulator Blend for Thermoelectrics. *Advanced Science* **2017,** *4* (1), 1600203.
60. Aziz, E. F.; Vollmer, A.; Eisebitt, S.; Eberhardt, W.; Pingel, P.; Neher, D.; Koch, N., Localized Charge Transfer in a Molecularly Doped Conducting Polymer. *Advanced Materials* **2007,** *19* (20), 3257-3260.
61. Un, H.-I.; Gregory, S. A.; Mohapatra, S. K.; Xiong, M.; Longhi, E.; Lu, Y.; Rigin, S.; Jhulki, S.; Yang, C.-Y.; Timofeeva, T. V.; Wang, J.-Y.; Yee, S. K.; Barlow, S.; Marder, S. R.; Pei, J., Understanding the Effects of Molecular Dopant on n-Type Organic Thermoelectric Properties. *Advanced Energy Materials* **2019,** *9* (24), 1900817.
62. Yamamoto, J.; Furukawa, Y., Electronic and Vibrational Spectra of Positive Polarons and Bipolarons in Regioregular Poly(3-hexylthiophene) Doped with Ferric Chloride. *The Journal of Physical Chemistry B* **2015,** *119* (13), 4788-4794.
63. Gregory, S. A.; Menon, A. K.; Ye, S.; Seferos, D. S.; Reynolds, J. R.; Yee, S. K., Effect of Heteroatom and Doping on the Thermoelectric Properties of Poly(3-alkylchalcogenophenes). *Advanced Energy Materials* **2018,** *8* (34), 1802419.
64. Lim, E.; Glaudell, A. M.; Miller, R.; Chabinyc, M. L., The Role of Ordering on the Thermoelectric Properties of Blends of Regioregular and Regiorandom Poly(3‐hexylthiophene). *Advanced Electronic Materials* **2019,** *5* (11).
65. Li, H.; DeCoster, M. E.; Ming, C.; Wang, M.; Chen, Y.; Hopkins, P. E.; Chen, L.; Katz, H. E., Enhanced Molecular Doping for High Conductivity in Polymers with Volume Freed for Dopants. *Macromolecules* **2019,** *52* (24), 9804-9812.
66. Imae, I.; Mashima, T.; Sagawa, H.; Komaguchi, K.; Ooyama, Y.; Harima, Y., In situ conductivity measurements of polythiophene partially containing 3,4-

ethylenedioxythiophene and 3-hexylthiophene. *Journal of Solid State Electrochemistry* **2015,** *19* (1), 71-76.
67. Ilavsky, J., Nika: software for two-dimensional data reduction. *Journal of Applied Crystallography* **2012,** *45* (2), 324-328.
68. Oosterhout, S. D.; Savikhin, V.; Zhang, J.; Zhang, Y.; Burgers, M. A.; Marder, S. R.; Bazan, G. C.; Toney, M. F., Mixing Behavior in Small Molecule:Fullerene Organic Photovoltaics. *Chemistry of Materials* **2017,** *29* (7), 3062-3069.
69. Menon, A. K.; Uzunlar, E.; Wolfe, R. M. W.; Reynolds, J. R.; Marder, S. R.; Yee, S. K., Metallo-organic n-type thermoelectrics: Emphasizing advances in nickel-ethenetetrathiolates. *Journal of Applied Polymer Science* **2017,** *134* (3).
70. Yee, S. K.; Coates, N. E.; Majumdar, A.; Urban, J. J.; Segalman, R. A., Thermoelectric power factor optimization in PEDOT:PSS tellurium nanowire hybrid composites. *Physical Chemistry Chemical Physics* **2013,** *15* (11), 4024-4032.

Table of Contents Figure:

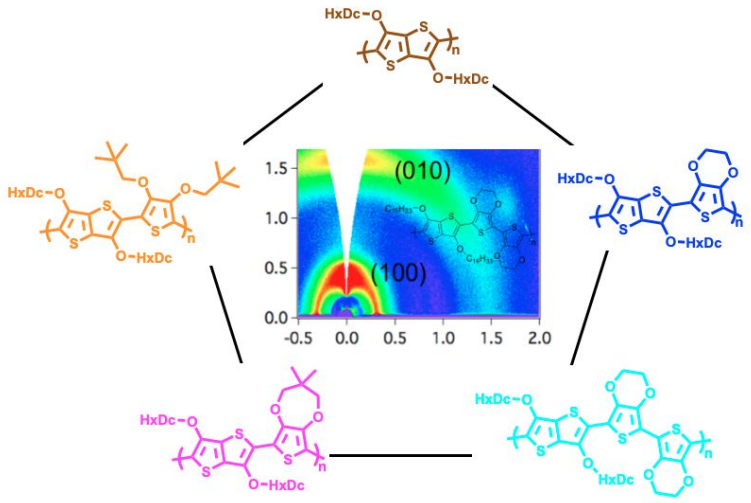

A new family of redox active dioxythienothiophene (DOTT) polymer are studied for their state ordering and doping susceptibility, along with their optical and electronic properties, ultimately yielding high electrical conductivities approaching 20 S/cm.